PHYSICAL REVIEW D **92,** 071301(R) (2015)

Vacuum birefringence in strong inhomogeneous electromagnetic fields

Felix Karbstein,[1,2] Holger Gies,[1,2] Maria Reuter,[1,3] and Matt Zepf[1,3,4]

[1]*Helmholtz-Institut Jena, Fröbelstieg 3, 07743 Jena, Germany*

[2]*Theoretisch-Physikalisches Institut, Abbe Center of Photonics, Friedrich-Schiller-Universität Jena, Max-Wien-Platz 1, 07743 Jena, Germany*

[3]*Institut für Optik und Quantenelektronik, Max-Wien-Platz 1, 07743 Jena, Germany*

[4]*Centre for Plasma Physics, School of Mathematics and Physics, Queen's University Belfast, Belfast BT7 1NN, United Kingdom*

(Received 8 July 2015; revised manuscript received 24 August 2015; published 26 October 2015)

Birefringence is one of the fascinating properties of the vacuum of quantum electrodynamics (QED) in strong electromagnetic fields. The scattering of linearly polarized incident probe photons into a perpendicularly polarized mode provides a distinct signature of the optical activity of the quantum vacuum and thus offers an excellent opportunity for a precision test of nonlinear QED. Precision tests require accurate predictions and thus a theoretical framework that is capable of taking the detailed experimental geometry into account. We derive analytical solutions for vacuum birefringence which include the spatio-temporal field structure of a strong optical pump laser field and an x-ray probe. We show that the angular distribution of the scattered photons depends strongly on the interaction geometry and find that scattering of the perpendicularly polarized scattered photons out of the cone of the incident probe x-ray beam is the key to making the phenomenon experimentally accessible with the current generation of FEL/high-field laser facilities.

DOI: 10.1103/PhysRevD.92.071301 PACS numbers: 12.20.Ds, 42.50.Xa, 12.20.−m

In strong electromagnetic fields the vacuum of quantum electrodynamics (QED) has peculiar properties. Fluctuations of virtual charged particles give rise to nonlinear, effective couplings between electromagnetic fields [1–3], which, e.g., can impact and modify the propagation of light, and even trigger the spontaneous decay of the vacuum via Schwinger pair production in electric fields [2,4,5]. Even though subject to high-energy experiments [6], so far the pure electromagnetic nonlinearity of the quantum vacuum has not been verified directly on macroscopic scales. In particular, the advent of petawatt class laser facilities has stimulated various proposals to probe quantum vacuum nonlinearities in high-intensity laser experiments; see the pertinent reviews [7–11] and references therein. One of the most famous optical signatures of vacuum nonlinearity in strong electromagnetic fields is vacuum birefringence [12–16], which is so far searched for in experiments using macroscopic magnetic fields [17,18]. A proposal to verify vacuum birefringence with the aid of high-intensity lasers has been put forward by [19], envisioning the combination of an optical high-intensity laser as pump and a linearly polarized x-ray pulse as probe; cf. also [20] who study x-ray diffraction by a strong standing electromagnetic wave. While [19] proposed the experimental scenario depicted in Fig. 1 for the first time, its theoretical description does not account for the possibility of momentum transfer from the pump field inhomogeneity—incorporating this in the present work entails an enhancement of the birefringence signal-to-noise ratio of several orders of magnitude.

In the present letter, we reanalyze vacuum birefringence in manifestly inhomogeneous fields, rephrasing the phenomenon in terms of a vacuum emission process [21]. We use new theoretical insights into photon propagation in slowly varying inhomogeneous electromagnetic fields [22], allowing us to overcome previous limitations and to calculate the angular divergence of the cross-polarized photons for the first time. Our study provides a new twist and perspective on the feasibility of future vacuum birefringence experiments. The key idea—so far completely unappreciated in this context—is to exploit the diffraction spreading of the outgoing signal photons. We detail on a realistic experimental setup combining a high-intensity laser system and an XFEL source as envisioned at the Helmholtz International Beamline for Extreme Fields (HIBEF) [23] at the European XFEL [24] at DESY. The

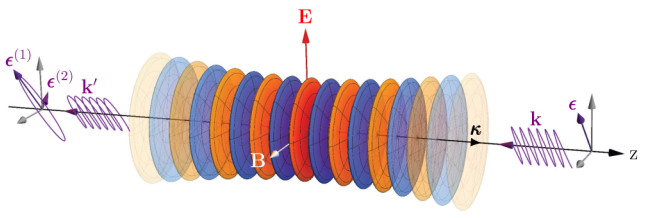

FIG. 1 (color online). Sketch of the pump-probe type scenario intended to verify vacuum birefringence. A linearly polarized optical high-intensity laser pulse—wavevector $\boldsymbol{\kappa}$, electric (magnetic) field $\mathbf{E}$ ($\mathbf{B}$)—propagates along the positive z axis. Its strong electromagnetic field couples to the charged particle-antiparticle fluctuations in the quantum vacuum, and thereby effectively modifies its properties to be probed by a counter-propagating x-ray beam (wavevector $\mathbf{k}$, polarization $\boldsymbol{\epsilon}$). Vacuum birefringence manifests itself in an ellipticity of the outgoing x-ray photons (wavevector $\mathbf{k}'$, polarization components along $\boldsymbol{\epsilon}^{(1)}$ and $\boldsymbol{\epsilon}^{(2)}$).

potential of diffraction effects for novel experimental signatures of quantum vacuum nonlinearity in other all-optical scenarios has been appreciated before; cf., e.g., [25–28].

From a theoretical perspective vacuum birefringence is most conveniently analyzed within the effective theory describing the propagation of macroscopic photon fields A^μ in the quantum vacuum. The corresponding effective action is $S_{\rm eff}[A,\mathcal{A}] = S_{\rm MW}[\mathbb{A}] + S_{\rm int}[A,\mathcal{A}]$, where $S_{\rm MW}[\mathbb{A}] = -\frac{1}{4}\int_x \mathbb{F}_{\mu\nu}(x)\mathbb{F}^{\mu\nu}(x)$ is the Maxwell action of classical electrodynamics, with $\mathbb{F}_{\mu\nu}$ denoting the field strength tensor of both the pump $\mathcal{A}^\mu$ and the probe A^μ field, i.e., $\mathbb{A}^\mu = \mathcal{A}^\mu + A^\mu$. The additional term $S_{\rm int}[A,\mathcal{A}] = -\frac{1}{2}\int_x\int_{x'} A_\mu(x)\Pi^{\mu\nu}(x,x'|\mathcal{A})A_\nu(x')$ encodes quantum corrections to probe photon propagation and vanishes for $\hbar \to 0$. All the effective interactions with the pump laser field are encoded in the photon polarization tensor $\Pi^{\mu\nu}(x,x'|\mathcal{A})$, evaluated in the $\mathcal{A}^\mu$ background. In momentum space, $\Pi^{\mu\nu}$ in inhomogeneous fields $\mathcal{A}_\mu(x)$ generically mediates between two independent momenta k^μ and k'^μ, i.e., $\Pi^{\mu\nu} \equiv \Pi^{\mu\nu}(k',k|\mathcal{A})$, This prevents a straightforward diagonalization of the probe photons' equation of motion, as possible in homogeneous fields [12,14], where $\Pi^{\mu\nu}$ only depends on the momentum transfer $(k'-k)^\mu$ due to translational invariance.

A particular convenient way to analyze vacuum birefringence in inhomogeneous fields is to phrase it as a vacuum emission process [21]. Viewing the pump and probe beams as macroscopic electromagnetic fields, and not resolving the individual photons constituting the beams, the vacuum subjected to these electromagnetic fields can be interpreted as a source term for outgoing photons. From this perspective, the induced photons correspond to the signal photons imprinted by the effective interaction of the pump and probe beams. For a linearly polarized x-ray beam brought into head-on collision with a linearly polarized optical high-intensity laser pulse, the induced x-ray signal generically encompasses photons whose polarization characteristics differ from the original probe beam. This results in induced photons polarized perpendicularly to the incident probe beam, which constitutes a signal of vacuum birefringence; cf. [29]. The outgoing x-ray beam, made up of the induced x-ray photons as well as the original probe beam which has traversed the pump laser pulse, then effectively picks up a tiny ellipticity.

We assume a linearly polarized x-ray probe beam, $A_\nu(x) = \frac{1}{2}\frac{\mathcal{E}}{\omega}\epsilon_\nu(\hat{k})e^{i\omega(\hat{k}x+t_0)-(\frac{\hat{k}x+t_0}{T/2})^2}$, of frequency $\omega = \frac{2\pi}{\lambda_{\rm probe}}$, peak field amplitude $\mathcal{E}$ and pulse duration T; $\epsilon_\nu(\hat{k})$ is the polarization vector of the beam and $\hat{k}^\mu = (1,\hat{\mathbf{k}})$, with unit wavevector $\hat{\mathbf{k}}$. In momentum space, the x-ray photon current generated by the pump and probe laser fields can be expressed as $j^\mu(k') = \frac{\sqrt{\pi}}{2}\frac{\mathcal{E}}{\omega}\frac{T}{2}\int\frac{d\tilde{\omega}}{2\pi}e^{-\frac{1}{4}(\frac{T}{2})^2(\tilde{\omega}-\omega)^2+it_0\tilde{\omega}}\Pi^{\mu\nu}(-k',\tilde{\omega}\,\hat{k}\,|\mathcal{A})\epsilon_\nu(\hat{k})$, and the associated single photon emission amplitude as $\mathcal{S}_{(p)}(k') = \frac{\epsilon^{*(p)}_\mu(\hat{k}')}{\sqrt{2\omega'}}j^\mu(k')$ [21], where the polarization vectors $\epsilon^{(p)}_\mu(\hat{k}')$, with $p \in \{1,2\}$, span the transverse polarizations of the induced photons of four-momentum $k'^\mu = \omega'(1,\hat{\mathbf{k}}')$. Employing $\mathcal{E} = \sqrt{2\langle I\rangle}$, with the probe mean intensity given by $\langle I\rangle = J\omega$, where $J \equiv \frac{N}{\sigma T}$ is the probe photon current density, i.e., the number N of incident frequency-ω photons per area σ and time interval T, the differential number of induced photons with polarization p determined with Fermi's golden rule, $d^3N^{(p)} = \frac{d^3k'}{(2\pi)^3}|\mathcal{S}_{(p)}(k')|^2$, becomes

$$d^3N^{(p)} = \frac{d^3k'}{(2\pi)^3}\left|\frac{\epsilon^{*(p)}_\mu(\hat{k}')}{\sqrt{2\omega'}}\mathcal{M}^{\mu\nu}(-k',k|\mathcal{A})\frac{\epsilon_\nu(\hat{k})}{\sqrt{2\omega}}\right|^2 J, \quad (1)$$

where we defined

$$\mathcal{M}^{\mu\nu}(-k',k|\mathcal{A}) = \sqrt{\pi}\frac{T}{2}\int\frac{d\tilde{\omega}}{2\pi}e^{-\frac{1}{4}(\frac{T}{2})^2(\tilde{\omega}-\omega)^2+it_0\tilde{\omega}} \times \Pi^{\mu\nu}(-k',\tilde{\omega}\,\hat{k}\,|\mathcal{A}). \quad (2)$$

For a plane-wave probe beam, recovered in the limit $T \to \infty$, we have $\mathcal{M}^{\mu\nu}(-k',k|\mathcal{A})|_{T\to\infty} = \Pi^{\mu\nu}(-k',k|\mathcal{A})$. Choosing $\boldsymbol{\epsilon}^{(p)}(\hat{k}')$ perpendicular to $\boldsymbol{\epsilon}(\hat{k})$, the modulus squared term in Eq. (1) can be interpreted as polarization flip probability [29].

We assume the high-intensity laser with normalized four wave vector $\hat{\kappa}^\mu = (1,\mathbf{e}_z)$ to be linearly polarized along $\mathbf{e}_E = (\cos\phi,\sin\phi,0)$ (cf. Fig. 1, where $\phi = 0$). The choice of the angle parameter ϕ fixes the directions of the electric and magnetic fields ($\mathbf{e}_B = \mathbf{e}_E|_{\phi\to\phi+\frac{\pi}{2}}$). Moreover, $k^\mu_\perp = (0,\mathbf{k} - (\hat{\boldsymbol{\kappa}}\cdot\mathbf{k})\hat{\boldsymbol{\kappa}})$ and $k'^\mu_\perp = k^\mu_\perp|_{\mathbf{k}\to\mathbf{k}'}$. For the following discussion it is convenient to turn to spherical coordinates and express the unit momentum vectors as $\hat{\mathbf{k}} = (\cos\varphi\sin\vartheta,\sin\varphi\sin\vartheta,-\cos\vartheta)$, such that $\hat{\mathbf{k}}|_{\vartheta=0} = -\mathbf{e}_z$, and likewise $\hat{\mathbf{k}}' = \hat{\mathbf{k}}|_{\varphi\to\varphi',\vartheta\to\vartheta'}$. Correspondingly, the polarization vectors can be expressed as $\boldsymbol{\epsilon}_\mu(\hat{k}) = (0,\mathbf{e}_{\varphi,\vartheta,\beta})$, with $\mathbf{e}_{\varphi,\vartheta,\beta} \equiv \sin\beta\,\hat{\mathbf{k}}|_{\vartheta=\frac{\pi}{2},\varphi\to\varphi+\frac{\pi}{2}} - \cos\beta\,\hat{\mathbf{k}}|_{\vartheta\to\vartheta+\frac{\pi}{2}}$, and $\boldsymbol{\epsilon}^{(p)}_\mu(\hat{k}') = (0,\mathbf{e}_{\varphi',\vartheta',\beta'})$. Without loss of generality $\boldsymbol{\epsilon}^{(1)}_\mu(\hat{k}')$ is fixed by a particular choice of β', and the perpendicular vector by $\boldsymbol{\epsilon}^{(2)}_\mu(\hat{k}') = \boldsymbol{\epsilon}^{(1)}_\mu(\hat{k}')|_{\beta'\to\beta'+\frac{\pi}{2}}$.

On shell, i.e., for $\hat{k}^2 = \hat{k}'^2 = 0$, $\Pi^{\mu\nu}$ in a linearly polarized, pulsed Gaussian laser beam reads (cf. Eq. (16) of [22])

$$\Pi^{\mu\nu}(-k',\tilde{\omega}\hat{k}) = -\omega'\tilde{\omega}\frac{\alpha}{\pi}\frac{1}{45}\frac{I_0}{I_{\rm cr}}g(k'-\tilde{\omega}\hat{k}) \times [4(\hat{k}'\hat{F})^\mu(\hat{k}\hat{F})^\nu + 7(\hat{k}'^*\hat{F})^\mu(\hat{k}^*\hat{F})^\nu], \quad (3)$$

where $g(k'-\tilde{\omega}\,\hat{k}) = \int_x e^{-i(k'-\tilde{\omega}\,\hat{k})x}g(x)$ is the Fourier transform of the normalized intensity profile of the pump laser in position space, $g(x) = I(x)/I_0$, with peak intensity I_0;

$\alpha = \frac{e^2}{4\pi} \simeq \frac{1}{137}$, and $I_{\rm cr} = (\frac{m^2}{e})^2 \approx 4.4 \times 10^{29} \frac{\rm W}{\rm cm^2}$. Here, the tensor structure is expressed in terms of $(\hat{k}\,\hat{F})^\mu = \varepsilon_1^\mu(\hat{k})\cos\phi + \varepsilon_2^\mu(\hat{k})\sin\phi$ and $(\hat{k}^*\hat{F})^\mu = (\hat{k}\,\hat{F})^\mu|_{\phi\to\phi+\frac{\pi}{2}}$, with $\varepsilon_1^\mu(\hat{k}) = (-\hat{k}_{\rm x}, \hat{\kappa}\hat{k}, 0, -\hat{k}_{\rm x})$ and $\varepsilon_2^\mu(\hat{k}) = (-\hat{k}_{\rm y}, 0, \hat{\kappa}\hat{k}, -\hat{k}_{\rm y})$. The polarization dependence of the induced photon signal (1) is encoded in the tensor structure in Eq. (3) contracted with the polarization vector of the probe beam and $\epsilon_\mu^{*(p)}(\hat{k}')$,

$$\epsilon_\mu^{*(p)}(\hat{k}')[4(\hat{k}'\hat{F})^\mu(\hat{k}\,\hat{F})^\nu + 7(\hat{k}'^*\hat{F})^\mu(\hat{k}^*\hat{F})^\nu]\epsilon_\nu(\hat{k}) = (1+\cos\vartheta')(1+\cos\vartheta)[4\cos\gamma'\cos\gamma + 7\sin\gamma'\sin\gamma], \tag{4}$$

where $\gamma = \varphi - \beta - \phi$ and $\gamma' = \varphi' - \beta' - \phi$. Equation (4) depends on the direction (φ, ϑ) and polarization (β) of the probe, the polarization of the pump (ϕ), as well as the emission direction (φ', ϑ') and polarization (β') of the induced photons.

Combining Eqs. (1)–(4), we obtain

$$\mathrm{d}^3N^{(p)} = \frac{\mathrm{d}^3k'}{(2\pi)^3}\frac{1}{\pi}\frac{\omega'}{\omega}\left(\frac{\alpha}{90}\frac{I_0}{I_{\rm cr}}\frac{T}{2}\right)^2(1+\cos\vartheta')^2(1+\cos\vartheta)^2 \times [4\cos\gamma'\cos\gamma + 7\sin\gamma'\sin\gamma]^2 \times \left|\int\frac{\mathrm{d}\tilde{\omega}}{2\pi}\mathrm{e}^{-\frac{1}{4}(\frac{T}{2})^2(\tilde{\omega}-\omega)^2 + it_0\tilde{\omega}}\tilde{\omega}\, g(k' - \tilde{\omega}\,\hat{k})\right|^2 J. \tag{5}$$

The total number of induced photons is obtained upon summation over the two photon polarizations p, i.e., $\sum_p \mathrm{d}^3N^{(p)}$. It can be inferred from Eq. (5) by substituting $[4\cos\gamma'\cos\gamma + 7\sin\gamma'\sin\gamma]^2 \to [16 + 33\sin^2\gamma]$.

So far our considerations were valid for arbitrary collision geometries of pump and probe. Subsequently, we stick to counter-propagating pump and probe beams, i.e., $\hat{k}^\mu = (1, -\mathbf{e}_{\rm z})$, as typically adopted in proposals for all-optical vacuum birefringence experiments [19] to maximize the overall factor of $(1+\cos\vartheta)^2|_{\vartheta=0} = 4$ in Eq. (5). In this limit it is convenient to set $\varphi = 0$, such that $\epsilon_\mu(\hat{k}) = (0, -\cos\beta, \sin\beta, 0)$. Besides, we assume $t_0 = 0$, such that the two laser pulses have an optimal temporal overlap and the effect is maximized. We adopt the standard choice $\beta = \frac{\pi}{4} - \phi$ (cf. [19]) for scenarios aiming at the detection of vacuum birefringence in a high-intensity laser experiment, implying that the polarization vector of the incident probe photons forms an angle of $\frac{\pi}{4}$ with respect to both the electric and magnetic field vectors of the pump; see Fig. 1. This ensures an equal overlap with the two photon polarization eigenmodes featuring different phase velocities in constant crossed and plane wave backgrounds. Note that the intensity profile of a linearly polarized, focused Gaussian laser pulse (frequency $\Omega = \frac{2\pi}{\lambda}$, beam waist w_0, pulse duration τ and phase φ_0), depending on the longitudinal (z) as well as the transverse (x, y) coordinates, is given by [30]

$$\mathfrak{g}(x) = \left[\mathrm{e}^{-\frac{(z-t)^2}{(\tau/2)^2}}\frac{w_0}{w(z)}\mathrm{e}^{-\frac{x^2+y^2}{w^2(z)}} \times \cos\left(\Omega(z-t) + \frac{x^2+y^2}{w^2(z)}\frac{z}{z_R} - \arctan\left(\frac{z}{z_R}\right) + \varphi_0\right)\right]^2, \tag{6}$$

with $w(z) = w_0\sqrt{1+(\frac{z}{z_R})^2}$ and Rayleigh range $z_R = \frac{\pi w_0^2}{\lambda}$.

In this paper, we consider three generic cases (cf. Fig. 2), namely (a) the radius of the x-ray probe beam is significantly smaller than the beam waist of the pump, (b) the probe beam radius is substantially larger than the beam waist of the pump [31], and (c) an asymmetric x-ray beam profile which is substantially smaller than the beam waist of the pump laser in one, and larger in the other transverse direction.

To tackle case (a) theoretically, we assume that the radius of the probe beam is so tiny that basically all probe photons propagate on the beam axis of the pump laser beam where the laser field becomes maximum. To this end, for $g(x)$ we adopt the on-axis profile of a focused Gaussian laser pulse, $g(x) = \mathfrak{g}(x)|_{x=y=0}$, i.e., do not account for the transverse structure of the beam. Correspondingly, the transverse momentum components remain unaffected and we have $\hat{\mathbf{k}}' = \hat{\mathbf{k}} = -\mathbf{e}_{\rm z}$, implying that the photons carrying the birefringence signal will be propagating in the direction of the original probe beam, and we can set $\varphi' = 0$. This kinematic restriction requires $\omega' = |k_{\rm z}'|$, but allows for $k_{\rm z}' \neq k_{\rm z}$ and $\omega' \neq \omega$. In the evaluation of Eq. (5) we can then make use of the homogeneity in the transverse directions, implying $g(k' - \tilde{\omega}\,\hat{k}) \sim (2\pi)^2\delta^{(2)}(k_\perp)$, and $\int_{k_\perp}\mathrm{d}^3N^{(p)} \sim J\sigma = \frac{N}{T}$.

Conversely, for case (b), where the probe inherently senses the transverse structure of the pump, such that in general $k'^\mu \neq k^\mu$, we take into account the full intensity profile of a focused Gaussian laser pulse, i.e., adopt $g(x) = \mathfrak{g}(x)$.

For case (c) we do not account for the transverse structure of the Gaussian beam along one direction, say y, but fully take it into account in x direction. Hence, we adopt $g(x) = \mathfrak{g}(x)|_{y=0}$, implying $k_{\rm y}' = k_{\rm y}$, but generically $k'^\mu \neq k^\mu$ for $\mu \in \{0,1,3\}$. Here, we have $g(k' - \tilde{\omega}\,\hat{k}) \sim (2\pi)\delta(k_{\rm y})$, such that $\int_{k_{\rm y}}\mathrm{d}^3N^{(p)} \sim JL_{\rm y} = \frac{N}{TL}$, with $L \equiv L_{\rm x}$.

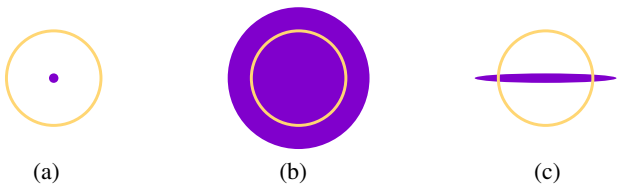

FIG. 2 (color online). Pictogram of the three different cases (a)–(c) considered in this paper. The circle (orange) is the cross section of the pump beam at its waist, and the filled circle/ellipse (purple) is the cross section of the probe beam.

As demonstrated below, in all of the cases (a)–(c) the induced x-ray photons are emitted in directions $\hat{\mathbf{k}}'$ very close to the propagation direction $\hat{\mathbf{k}}$ of the probe beam, and hence fulfill $\vartheta' \ll 1$. Within at most a few tens of μrad the signal falls off rapidly to zero, and we have $\boldsymbol{\epsilon}_\mu^{(p)}(\hat{k}') = (0, -\cos(\beta' - \varphi'), \sin(\beta' - \varphi'), 0) + \mathcal{O}(\vartheta')$. This implies that one can decompose the induced photon signal into photons polarized parallel, $\boldsymbol{\epsilon}_\mu^{(\parallel)}(\hat{k}')$ ($\beta' = \frac{\pi}{4} - \phi + \varphi'$), and perpendicular, $\boldsymbol{\epsilon}_\mu^{(\perp)}(\hat{k}')$ ($\beta' = \frac{3\pi}{4} - \phi + \varphi'$), to the probe. In turn, Eq. (5) becomes φ' independent, and $\int \mathrm{d}\varphi' \to 2\pi$. The term $[4\cos\gamma'\cos\gamma + 7\sin\gamma'\sin\gamma]^2$ encoding the polarization dependence in Eq. (5), becomes $\frac{121}{4}$ ($\frac{9}{4}$) for the $\parallel$ ($\perp$) polarization mode. The $\perp$-polarized photons constitute the birefringence signal [29].

To obtain realistic estimates for the numbers of induced photons for a state-of-the-art laser system, we assume the pump laser to be of the 1 PW class (pulse energy $W = 30$ J, pulse duration $\tau = 30$ fs and wavelength $\lambda = 800$ nm) focused to $w_0 = 1$ μm. The associated peak intensity is $I_0 = 2\frac{0.86W}{\tau\pi w_0^2}$; the effective focus area contains 86% of the beam energy ($1/\mathrm{e}^2$ criterion). For the x-ray probe we choose $\omega = 12914$ eV, for which the presently most sensitive x-ray polarimeter [32] was benchmarked. The polarization purity of x-rays of this frequency can be measured to the level of 5.7×10^{-10}. Assuming also the probe beam to be well described as a focused Gaussian beam of waist r, its divergence is given by $\theta(r) = \frac{\lambda_{\mathrm{probe}}}{\pi r}$. Neglecting diffraction and curvature effects for the probe in the actual calculation is nevertheless well justified as long as $\mathrm{z}_{R,\mathrm{probe}} \gg \mathrm{z}_R$. Measuring r in units of w_0, i.e., $r = \rho w_0$, we have $\frac{\mathrm{z}_{R,\mathrm{probe}}}{\mathrm{z}_R} = \rho^2\frac{\omega}{\Omega}$, implying that $\mathrm{z}_{R,\mathrm{probe}} \geq \mathrm{z}_R$ for $\rho^2 \geq \frac{\Omega}{\omega}$. Generically, we find $\frac{\Omega}{\omega} < \mathcal{O}(10^{-3})$ [33].

We first focus on case (a), where $r \ll w_0$. In Fig. 3 we plot $\frac{T}{N}\frac{\mathrm{d}N^{(\perp)}}{\mathrm{d}k_\mathrm{z}'}$. Upon integration over k_z' we obtain

	T[fs]	$N^{(\perp)}/\frac{N}{T}[\frac{1}{\mathrm{fs}}]$	$N^{(\perp)}/N$
(a)	∞	1.12×10^{-10}	–
	500	1.10×10^{-10}	2.20×10^{-13}
	30	4.16×10^{-11}	1.39×10^{-12}

Keeping all other parameters fixed, these results can be rescaled as $(\frac{W[J]}{30})^2$ to any other pump laser energy. Note that even the maximum ratio $\frac{N^{(\perp)}}{N} \approx 1.39 \times 10^{-12}$ obtained here for $T = 30$ fs is too small to be confirmed experimentally with currently available x-ray polarization purity [32] (improvement by a factor of $\gtrsim$410 required).

As to be expected, in scenario (b) the numbers of induced photons are lower. In this case the probe senses the transverse structure of the focused pump, which results in outgoing x-ray photons with nonvanishing transverse momentum components. This can provide us with an additional handle to identify the induced photon signal

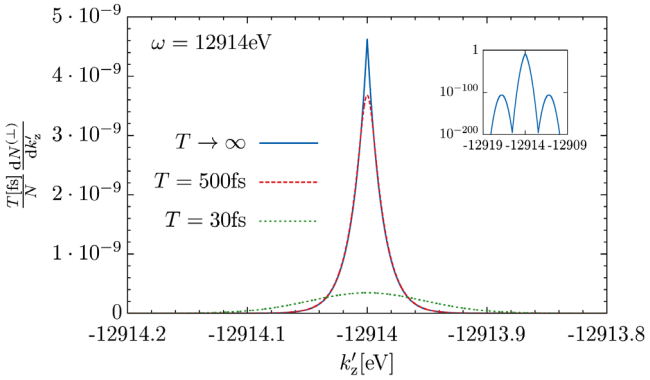

FIG. 3 (color online). Plot of $\frac{T}{N}\frac{\mathrm{d}N^{(\perp)}}{\mathrm{d}k_\mathrm{z}'}$ for case (a) as a function of k_z'. The induced photon signal is peaked at $k_\mathrm{z}' = -\omega$ and rapidly falls off to zero. We depict results for different probe pulse durations T. The inlay shows a plot of the same quantity for $T \to \infty$ ($\varphi_0 = 0$) over a wider frequency range, adopting a logarithmic scale. Here, the strongly suppressed contributions to be associated with frequencies $\approx\omega \pm 2\Omega$ are clearly visible.

as we can search for $\perp$-polarized photons emitted outside $\theta(r)$ (cf. Fig. 4), where the demand on the polarization purity is significantly lower due to the low photon background. Denoting the number of $\perp$-polarized photons emitted outside $\theta(r)$ as $N^{(\perp)}_{>\theta(r)}$, we consider probe beams of width $r = \rho w_0$ and exemplarily show results for $\rho = 3$. Identifying the cross section of the x-ray probe with $\sigma = \pi(\rho w_0)^2$, for case (b) we infer $N^{(\perp)}/N \sim \rho^{-2}$ and

	T[fs]	$N^{(\perp)}/J[\frac{1}{\mu\mathrm{m}^2\ \mathrm{fs}}]$	$N^{(\perp)}/N$	$N^{(\perp)}_{>\theta(3w_0)}/N^{(\perp)}$
(b)	∞	1.79×10^{-10}	–	63.1%
	500	1.52×10^{-10}	$9.68 \times 10^{-14}/\rho^2$	72.1%
	30	3.66×10^{-11}	$3.88 \times 10^{-13}/\rho^2$	88.1%

Analogously, setting $L = 2\rho w_0$ for case (c) we find $N^{(\perp)}/N \sim \rho^{-1}$ and

	T[fs]	$N^{(\perp)}/\frac{N}{TL}[\frac{1}{\mu\mathrm{m fs}}]$	$N^{(\perp)}/N$	$N^{(\perp)}_{>\theta(3w_0)}/N^{(\perp)}$
(c)	∞	6.38×10^{-11}	–	51.1%
	500	6.11×10^{-11}	$1.22 \times 10^{-13}/\rho$	52.6%
	30	1.95×10^{-11}	$6.50 \times 10^{-13}/\rho$	61.7%

Hence, especially for large probe beam widths ($\rho > 1$), case (c) is experimentally favored as it provides for the largest number of signal photons outside $\theta(\rho w_0)$. Finally, we demonstrate that the $\perp$-polarized photons emitted outside $\theta(r)$ can be measured with state-of-the-art technology. To do this, we stick to case (c) with $T = 30$ fs and $\rho = 3$. The number of $\perp$-polarized photons scattered in directions $\vartheta' \geq \vartheta_{\mathrm{min}}$ can be estimated from Fig. 4 as $N^{(\perp)}_{>\vartheta_{\mathrm{min}}} \approx N^{(\perp)}[1 - \mathrm{erf}(\sqrt{1.13}\frac{\vartheta_{\mathrm{min}}}{\theta(w_0)})]$, where erf(.) is the error function. Similarly, the number of probe photons outside ϑ_{min} is $N_{>\vartheta_{\mathrm{min}}} = N[1 - \mathrm{erf}(\sqrt{2}\frac{\vartheta_{\mathrm{min}}}{\theta(3w_0)})]$. Herefrom,

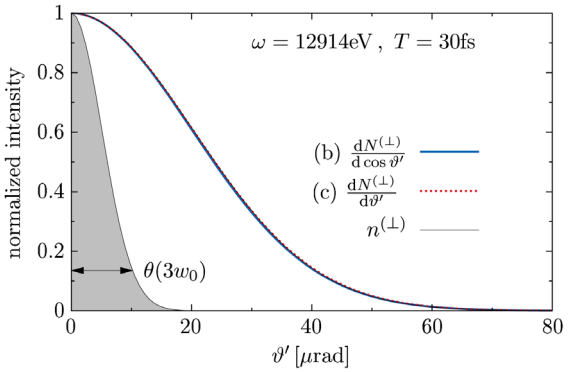

FIG. 4 (color online). Plot of $\frac{dN^{(\perp)}}{d\cos\vartheta'} \equiv 2\pi \int_0^\infty d\omega' \omega'^2 \frac{d^3N^{(\perp)}}{d^3k'}$ for case (b) and $\frac{dN^{(\perp)}}{d\vartheta'} \equiv \int dk'_z \int_0^\infty d\omega' \omega' \frac{d^3N^{(\perp)}}{d^3k'}$ for case (c) as a function of the emission angle ϑ'. For $T = 30$ fs the two curves basically fall on top of each other, and are well approximated by $n^{(\perp)}(\xi) = \exp\{-\xi(\frac{\vartheta'}{\theta(w_0)})^2\}$ with $\xi = 1.13$. This profile is compatible with naive expectations: From $N^{(\perp)} \sim I^2$ and $\omega' \approx \omega$ we might have guessed $dN^{(\perp)} \sim n^{(\perp)}(\xi = 1)$. For comparison, the intensity profile of a Gaussian probe beam of divergence $\theta(3w_0)$ is depicted in gray.

we can determine the value of $\vartheta_{\min}$ for which the ratio $\frac{N^{(\perp)}}{N}|_{>\vartheta_{\min}}$ exceeds the polarization purity of the presently best x-ray polarimeter. We find that this is achieved for $\vartheta_{\min} \geq 19.50\ \mu$rad. For this choice we have $\frac{N^{(\perp)}_{>\vartheta_{\min}}}{N} \gtrsim 7.37 \times 10^{-14}$, such that, assuming the probe pulse to comprise $N = 10^{12}$ photons and a repetition rate of 1 Hz, we expect to detect $N^{(\perp)}_{>\vartheta_{\min}} \approx 265$ $\perp$-polarized photons per hour. Reducing the pulse energy of the pump to $W = 3$ J, while keeping all other parameters fixed, results in the requirement $\vartheta_{\min} \geq 25.10\ \mu$rad, for which $\frac{N^{(\perp)}_{>\vartheta_{\min}}}{N} \gtrsim 4.77 \times 10^{-16}$. Due to the lower pulse energy, the repetition rate can be increased to 10 Hz, yielding $N^{(\perp)}_{>\vartheta_{\min}} \approx 17$ $\perp$-polarized photons per hour.

In conclusion, we have demonstrated that vacuum birefringence can be verified experimentally with state-of-the-art technology. The key idea to making this phenomenon experimentally accessible is to exploit the scattering of $\perp$-polarized photons out of the cone of the incident probe x-ray beam. For the treatment of realistic laser fields, it is computationally efficient to reformulate vacuum birefringence as vacuum emission [21], and employ new theoretical insights into photon propagation in slowly varying inhomogeneous fields [22]. We are optimistic that our study can pave the way for an experimental verification of vacuum birefringence in an all-optical experiment.

We acknowledge support by the DFG (SFB-TR18) and EPSRC.

[1] H. Euler and B. Kockel, Naturwissenschaften **23**, 246 (1935).
[2] W. Heisenberg and H. Euler, Z. Phys. **98**, 714 (1936); English translation available at, arXiv:physics/0605038.
[3] V. Weisskopf, Kong. Dans. Vid. Selsk., Mat.-fys. Medd. **XIV**, 6 (1936).
[4] F. Sauter, Z. Phys. **69**, 742 (1931).
[5] J. S. Schwinger, Phys. Rev. **82**, 664 (1951).
[6] S. Z. Akhmadaliev *et al.*, Phys. Rev. C **58**, 2844 (1998); Phys. Rev. Lett. **89**, 061802 (2002).
[7] W. Dittrich and H. Gies, Springer Tracts Mod. Phys. **166**, 1 (2000).
[8] M. Marklund and J. Lundin, Eur. Phys. J. D **55**, 319 (2009).
[9] G. V. Dunne, Eur. Phys. J. D **55**, 327 (2009).
[10] T. Heinzl and A. Ilderton, Eur. Phys. J. D **55**, 359 (2009).
[11] A. Di Piazza, C. Muller, K. Z. Hatsagortsyan, and C. H. Keitel, Rev. Mod. Phys. **84**, 1177 (2012).
[12] J. S. Toll, Ph. D. thesis, Princeton University, 1952.
[13] R. Baier and P. Breitenlohner, Acta Phys. Austriaca **25**, 212 (1967); Nuovo Cimento B **47**, 117 (1967).
[14] Z. Bialynicka-Birula and I. Bialynicki-Birula, Phys. Rev. D **2**, 2341 (1970).
[15] S. L. Adler, Ann. Phys. (N.Y.) **67**, 599 (1971).
[16] G. L. Kotkin and V. G. Serbo, Phys. Lett. B **413**, 122 (1997).
[17] G. Cantatore (PVLAS Collaboration), Lect. Notes Phys. **741**, 157 (2008); E. Zavattini *et al.* (PVLAS Collaboration), Phys. Rev. D **77**, 032006 (2008); F. Della Valle *et al.*, New J. Phys. **15**, 053026 (2013).
[18] P. Berceau, R. Battesti, M. Fouche, and C. Rizzo, Can. J. Phys. **89**, 153 (2011); P. Berceau, M. Fouche, R. Battesti, and C. Rizzo, Phys. Rev. A **85**, 013837 (2012); A. Cadene, P. Berceau, M. Fouche, R. Battesti, and C. Rizzo, Eur. Phys. J. D **68**, 16 (2014).
[19] T. Heinzl, B. Liesfeld, K. U. Amthor, H. Schwoerer, R. Sauerbrey, and A. Wipf, Opt. Commun. **267**, 318 (2006).
[20] A. Di Piazza, K. Z. Hatsagortsyan, and C. H. Keitel, Phys. Rev. Lett. **97**, 083603 (2006).
[21] F. Karbstein and R. Shaisultanov, Phys. Rev. D **91**, 113002 (2015).
[22] F. Karbstein and R. Shaisultanov, Phys. Rev. D **91**, 085027 (2015).
[23] cf. the HIBEF website, http://www.hzdr.de/db/Cms?pOid=35325&pNid=3214.
[24] cf. the XFEL website, http://www.xfel.eu.
[25] E. Lundstrom, G. Brodin, J. Lundin, M. Marklund, R. Bingham, J. Collier, J. T. Mendonca, and P. Norreys, Phys. Rev. Lett. **96**, 083602 (2006).

[26] B. King, A. Di Piazza, and C. H. Keitel, Nat. Photonics **4**, 92 (2010); Phys. Rev. A **82**, 032114 (2010).

[27] D. Tommasini and H. Michinel, Phys. Rev. A **82**, 011803 (2010).

[28] B. King and C. H. Keitel, New J. Phys. **14**, 103002 (2012).

[29] V. Dinu, T. Heinzl, A. Ilderton, M. Marklund, and G. Torgrimsson, Phys. Rev. D **89**, 125003 (2014); Phys. Rev. D **90**, 045025 (2014).

[30] A. E. Siegman, *Lasers*, 1st ed. (University Science Books, Sausalito, CA, 1986); B. E. A. Saleh and M. C. Teich, *Fundamentals of Photonics*, 1st ed. (John Wiley & Sons, New York, 1991).

[31] The beam waist w_0 is assumed to be an adequate measure of the pump's beam radius as the intensity falls off rapidly outside the focus.

[32] B. Marx *et al.*, Opt. Commun. **284**, 915 (2011); Phys. Rev. Lett. **110**, 254801 (2013).

[33] See Supplemental Material at http://link.aps.org/supplemental/10.1103/PhysRevD.92.071301 for the explicit formulas used to obtain the explicit numerical results presented in the following.